# Feasibility of Plasma Spraying in Developing MMC Coatings: Modeling the Heating of Coated Powder Particles

**Marios D. Demetriou**
**Adrienne S. Lavine**
**Nasr M. Ghoniem**

Mechanical & Aerospace Engineering Department,
University of California, Los Angeles,
Los Angeles, CA 90095-1597

*Coated powder particles composed of a ceramic core and a metallic coating are being considered for plasma spray applications. The goal of using these powders is to produce particulate-reinforced metal-matrix composite coatings. In this work, the feasibility of plasma spray processing in producing these composite coatings is evaluated. A numerical model is presented to analyze the in-flight thermal behavior and physical state of moderate-size particles (10–30 μm radius) in arc-jet DC plasma under low loading conditions. The pairs of materials for the base and coating that are considered in this work are WC-Co, SiC-Ni, and SiC-Al. The plasma was taken to be atmospheric argon plasma. The study suggests that plasma processing is capable of melting the coating without excessive evaporation while retaining the base in the solid state over a range of particle sizes and base/coating proportions. Hence plasma processing appears suitable to develop particulate-reinforced metal-matrix composite coatings.*
[DOI: 10.1115/1.1403742]

## 1 Introduction

Coated, or encapsulated, powders have been in development and commerce for several decades. Metal-coated powders have been in development since fluidized bed coating of powders was initially developed for the production of nuclear fuel pellets for gas-cooled reactors in the late 1950's and early 1960's. Two different methods are currently being used for the preparation of metal-coated powders: sulfimate-plating baths (the older method), and chemical vapor deposition from carbonyl or other organometallic precursors carried out in a fluidized bed, which produces more uniformly coated fine particulates. Coated powder technology has only recently been placed into large-scale commercial products, consisting of coated fillers for electrostatic shielding (500,000 lbs./year), and thermal spray products (300,000 lbs./year). To date, no modeling work has been carried out to establish the feasibility of plasma spray technology in producing composite coatings using coated powders.

Metals reinforced with rigid ceramic particles that do not enter into reaction with the matrix are referred to as discontinuously reinforced metal-matrix composites. The use of coated powder particles (composed of a ceramic core and a metallic coating) in the plasma spraying process has the potential for producing discontinuously reinforced metal-matrix composite coatings. These composites display better structural efficiency, reliability, and mechanical performance over their matrix material [1]. In a metal matrix composite, the reinforcement also acts to change the micro-contact geometry of mating surfaces and, thus, the wear mechanisms, resulting in improved tribological behavior over the monolithic counterpart [2]. Furthermore, particulate-reinforced metal-matrix composites are attractive because they exhibit near isotropic properties when compared to the continuously reinforced counterpart, besides providing the additional advantage of being machinable and workable [1]. They can provide effective means of wear protection in many fields of industry where severe wear and high working forces are present at high temperature, especially if stiffness and low weight are primary considerations [1,3].

Contributed by the Manufacturing Engineering Division for publication in the JOURNAL OF MANUFACTURING SCIENCE AND ENGINEERING. Manuscript received September 1999; revised January 2001. Associate Editor: M. Ohadi.

Tungsten carbide (WC) presents one of the best resistances to softening induced by temperature increase. Tungsten carbide films are very hard but also very brittle. Addition of cobalt can contribute to the toughness and therefore improve the compromise between hardness and toughness of the films [3]. Moreover, it can serve as a binder and as a crack inhibitor. Tungsten carbide-cobalt (WC-Co) cermet composites are widely used in industry for cutting and boring tools and in hard facing applications.

Silicon carbide (SiC) whiskers or particulates are commonly used as reinforcement in aluminum-based alloys as a result of their high modulus, high hardness, low cost, easy availability, and limited reactivity with aluminum. The advantages of the resulting composite include dramatic increase in modulus, proof strength, and ultimate strength, increased elevated temperature strength, increased abrasion resistance, improved fatigue crack resistance, and improved creep rupture properties [1]. The combination of properties offered by SiC-Al metal matrix composites shows potential for applications in automotive, aerospace, and defense industries.

Silicon carbide/nickel composite coatings are candidates for replacing cylinder liners, as the improved tribological properties of the composite make it suitable to coat the lubricated reciprocating contacts [2].

Quantitative knowledge of the thermal behavior of a particle in a plasma flame is essential in optimizing the process variables (such as current, voltage, gas flow rate, powder feed rate, target distance, etc.) to achieve uniform heating to the liquid state. Various researchers have previously modeled the thermal behavior of a single homogeneous particle in plasma. Fiszdon [4] accounted for non-uniform plasma conditions for a particle traveling along the centerline of the plasma reactor. Assuming steady plasma, Lee et al. [5] accounted for varying plasma properties and temperature jump, and investigated the effects of relaxation time, radiation transport, internal conduction, particle shape, and particle charging. Jog and Huang [6] modeled a single particle in steady plasma, and investigated the effects of gas ionization and particle charging by incorporating a model for production and recombination of electrons and ions. Wan et al. [7] accounted for the actual off-centerline trajectory of the particle by making use of the LAVA code to predict, under given power, the 3-D plasma gas field.

  

The primary objective of this work is to assess the suitability of the plasma spray process in developing particulate-reinforced metal-matrix composites. In other words, the aim is to determine whether under conventional plasma processing conditions this process is capable of melting the coating of these powder particles, without excessive evaporation, while retaining the base in the solid state. The coated particles WC-Co, SiC-Al, and SiC-Ni were considered, injected in an argon arc-jet DC plasma. The effect of the particle size and base/coating relative amounts on melting and evaporation of the coating was investigated. Furthermore, the feasibility of the process is assessed by determining a particle size range that for a given base/coating relative amount would result, under the given conditions, in an entirely molten coating without significant evaporative losses at the end of the particle flight.

To carry out this investigation, a model was developed based primarily on the work of the authors mentioned above. It employs features from the current literature to adequately model the in-flight thermal behavior of moderate-size particles (10–30 $\mu$m radius) under low loading conditions. Moreover, the enthalpy method was introduced to treat the phase change problem. This method eliminates the need to accurately track moving phase boundaries in modeling phase change problems such as melting or solidification.

## 2 The Model

The problem consists of two coupled sub-problems: The first is the plasma-particle interactions, which involves the exchange of heat, mass, and momentum between the plasma and the particle. In this part, the theories, correlations, and corrections of previous studies were adopted to model plasma thermal transport to moderate-size particles (10–30 $\mu$m radius) under low loading conditions. The second problem is the thermal model for the particle, which involves heating, melting and evaporation of the coating of the particle. The enthalpy method was employed to treat the phase change due to its attractive simplicity and sufficient accuracy. The two sub-problems are coupled together through the particle radius and surface temperature.

The model was validated by comparing it against the model presented by Chen and Pfender [8] for alumina and tungsten particles entrained in steady argon plasma and the one presented by Lee et al. [5] for tungsten particles also entrained in steady argon plasma. Under these conditions, the developed model is in excellent agreement with the previously established models.

**2.1 Plasma-Particle Interactions.** The model takes into account non-steady plasma conditions (assuming quasi-steady conditions) and makes use of the readily available steady-flow empirical correlations from the plasma heat transfer literature [9,10]. The turbulent eddies of the plasma flow may cause the particle to travel in off-centerline trajectories, as studied by Wan et al. [7]. However, Pfender and Lee [9] suggested that the range of dispersed particle motion is small for particles greater than 10 $\mu$m in turbulent jets, therefore the turbulent dispersion was neglected in this model and a centerline particle trajectory was assumed. As suggested by Lee et al. [5], the contribution of ion recombination becomes important only if frozen conditions prevail in the boundary layer, or if the molecular flow regime is approached. Since none of these conditions were encountered in the present study, the model neglects the effects of gas ionization and particle charging. Also, the simulation of a single particle could sufficiently represent the case of multi-particle injection under low loading conditions, for which the particle interactions with the plasma and between particles can be neglected. The detailed listing of the correlations used in this section can be found in the work of Demetriou et al. [11].

*Momentum Transfer.* The viscous drag force experienced by the particle is given by:

$$F_v = \frac{1}{2}\pi r_o^2 C_d \rho_g u_r |u_r| \tag{1}$$

where $r_o$ is the particle outer radius, $\rho_g$ is the gas density evaluated at the free-stream temperature, $u_r$ is the relative speed between the particle and the gas, and $C_d$ is the drag coefficient. The correlation for the drag coefficient was taken from Pfender and Lee [9], which takes into account property variation across the viscous boundary layer and corrects for velocity slip. The effects of thermophoresis and Basset history on the drag force were included but were found to be negligible as compared to viscous effects. The effect of blowing on droplet drag due to evaporation from the droplet surface was also neglected [12].

*Heat Transfer.* The convective heat flux out of the particle is given as follows:

$$q_{\text{conv}} = \frac{\text{Nu}\ k_f}{2r_o}(T_w - T_g) \tag{2}$$

where $T_w$ is the particle surface temperature, $T_g$ is the gas free-stream temperature, $k_f$ is the thermal conductivity of the gas evaluated at the mean film temperature and Nu is the Nusselt number. The correlation for the Nusselt number is taken from Young and Pfender [10]. This correlation takes into account the effect of varying properties across the thermal boundary layer due to temperature variation. It is corrected for temperature jump as suggested by Chen and Pfender [13]. Moreover, the heat transfer coefficient ($h = \text{Nu}k_f/2r_o$) is corrected for the effect of blowing as suggested by Mills [14].

Chen and Pfender [8] argue that the effect of radiation from the plasma to the particle is negligible compared to other heat transfer mechanisms. Therefore, the radiative flux leaving the surface of the particle accounts only for the particle radiative losses to the cooled wall confining the plasma, and is given by Lee et al. [5] as follows:

$$q_{\text{rad}} = \varepsilon\sigma T_w^4 \tag{3}$$

where $\varepsilon$ is the emissivity of the particle and $\sigma$ is the Stefan-Boltzmann constant.

The evaporative heat flux leaving the particle surface may be computed as follows:

$$q_{\text{evap}} = \dot{m}'' L_{\text{evap}} \tag{4}$$

where $L_{\text{evap}}$ is the latent heat of vaporization, and $\dot{m}''$ is the evaporative mass flux which can be determined from the solution to the mass transfer problem discussed below.

*Mass Transfer.* The evaporative mass flux can be obtained from the following expression:

$$\dot{m}'' = \frac{\text{Sh}\rho_f D_{vg}}{2r_o}\ln\left(\frac{1}{1-m_v}\right) \tag{5}$$

where $\rho_f$ is the gas density evaluated at the mean film temperature, $D_{vg}$ is the mass diffusivity of particle vapor in pure gas and is computed using the kinetic theory of gases [14], and $m_v$ is the mass fraction of particle vapor in the gas mixture which can be related to its partial pressure. The partial pressures were approximated using the Clausius-Clapeyron relation [14]. The Sherwood number, Sh, can be derived from a correlation analogous to the one for Nusselt number taken from Young and Pfender [10] by replacing Prandtl with Schmidt number. Because the effect of varying properties across the mass boundary layer due to temperature and composition variation has not been well documented, it will not be accounted for in this work. The effect of composition jump on mass transfer will also be neglected in this analysis.

**2.2 Thermal Model for the Particle.** The base (WC or SiC) is taken to be a high temperature ceramic that melts invariantly at a temperature close to the boiling temperature of the metal coating. It is of vital interest to keep the process well below the

boiling point of the coatings in order to retain some coating in the liquid state and build the MMC coating upon impingement with the target. Therefore it appears to be unnecessary to account for a phase transition of the base material, as it would not occur within the optimum particle temperature range for MMC coatings. Although the base and coating melting points are far apart, the two materials may react to form a eutectic at temperatures lower than the melting point of the metal coating. Hence, if sufficient interdiffusion takes place, liquid may first nucleate at the ceramic-metal interface, rather than at the outer boundary. This solid-state reaction would be initiated by solid-state diffusion, and since it is very slow as compared to heat diffusion, it is neglected. Although the solid-state reaction may not occur, dissolution of the carbide base into the liquid metallic coating may occur that could affect the heating and could lead to de-carburization of the powder. According to the study of Sobolev et al. [15], the dissolution process is expected to be limited by atom diffusion through the dissolution layer, and for the short time scales of the plasma spray process, the developed dissolution layer is expected to be too small for any significant de-carburization or any other thermal effect to take place.

The enthalpy method [16] is employed to treat the phase change problem. In the enthalpy method, the governing equations are reformulated in terms of the enthalpy. The advantages of this approach are that there are no conditions to be satisfied at the phase change boundary, and there is no need to accurately trace the phase change boundary.

*Mathematical Formulation.* For spherical geometry with conduction only in the radial direction, the governing equations for each physical state reduce to a single equation:

$$\rho_j \frac{\partial H}{\partial t} = \frac{1}{r^2}\frac{\partial}{\partial r}\left[ r^2 \left( k_j(T)\frac{\partial T}{\partial r}\right)\right] \tag{6}$$

where $H$ and $T$ are enthalpy and temperature respectively, $t$ is time, $r$ is the radial coordinate in the spherical particle, $\rho$ and $k$ are the particle density (assumed independent of temperature) and thermal conductivity respectively. There are two boundary conditions associated with the temperature field described by the above equation:

$$\left.\frac{\partial T}{\partial r}\right|_{r=0} = 0 \tag{7}$$

$$\left.\left( k_j(T)\frac{\partial T}{\partial r}\right)\right|_{r=r_o} = q_{\text{conv}} + q_{\text{rad}} + q_{\text{evap}} \tag{8}$$

The initial condition associated with Eq. (6) is given by:

$$H(t=0) = c_j(T_i - T_{\text{ref}}) \tag{9}$$

where $c$ is the specific heat, $T_i$ is the initial temperature and $T_{\text{ref}}$ is arbitrary and determines the enthalpy datum.

All particle properties used in Eqs. (6)–(9) above, $k$, $\rho$, and $c$, are step-like functions of the location $r$ within the particle because the particle material is taken to be inhomogeneous (consisting of a homogeneous base and a homogeneous coating). Therefore, the index $j$ takes the value of the base property in the base region and the value of the coating property in the coating region, i.e.,

$$j \equiv \begin{cases} b & r < R_i \\ c & r > R_i \end{cases}$$

where $R_i$ is the radius defining the base/coating interface.

Assuming constant specific heat in each of the physical states of the particle, the reference enthalpies for the coating material are defined as follows:

$$H_{\text{SM}} = c_{sc}(T_{\text{melt}} - T_{\text{ref}}),$$

$$H_{\text{LM}} = H_{\text{SM}} + L_{\text{fus}},$$

where $c_{sc}$ and $c_{lc}$ refer to the specific heat of the solid and liquid respectively, $T_{\text{melt}}$ is the melting temperature, and $L_{\text{fus}}$ is the latent heat of fusion.

The temperature is related to the enthalpy as follows:
If $r < R_i$ (base region)

$$T = T_{\text{ref}} + H/c_b \tag{10a}$$

or else, if $r > R_i$ (coating region)

$$T = \begin{cases} T_{\text{ref}} + H/c_{sc} & H < H_{\text{SM}} \\ T_{\text{melt}} & H_{\text{SM}} \leqslant H < H_{\text{LM}} \\ T_{\text{melt}} + (H - H_{\text{LM}})/c_{lc} & H \geqslant H_{\text{LM}} \end{cases} \tag{10b}$$

where equilibrium melting is assumed.

The model presented above takes into account the effect of internal conduction resistance, although for certain materials, sizes, and conditions internal resistance can be neglected and a lumped thermal capacity model could be used.

*Transient Temperature Distribution.* The problem formulated in the enthalpy domain [Eqs. (6)–(9)] is discretized in space and time using an explicit finite difference scheme based on the control volume formulation. The initial enthalpy of each control volume is computed using Eq. (9). The enthalpy change at every time step for each control volume is then computed using the finite difference form of Eqs. (6)–(8), hence the transient enthalpy distribution is formulated. In turn, using Eq. (10), the transient enthalpy distribution is transformed to the transient temperature distribution.

*Moving Phase Boundaries.* The solid-liquid phase boundary is traced by tracking the enthalpy of the material. The solid-liquid boundary will be contained in the control volume whose enthalpy lies in the region $H_{SM} \leqslant H < H_{LM}$. The exact location of the boundary can be obtained by defining the solid fraction in that control volume. Assuming small enthalpy gradients in the vicinity of the melting location, the solid fraction can be approximated as:

$$\psi \cong \frac{H_{\text{LM}} - H}{H_{\text{LM}} - H_{\text{SM}}} = \frac{H_{\text{LM}} - H}{L_{\text{fus}}} \tag{11}$$

For a solid-liquid boundary lying within the $n$th control volume, the radius of the solid-liquid boundary can then be computed from

$$r_i^3 = r_n^3 \psi + r_{n-1}^3 (1 - \psi) \tag{12}$$

The location of the liquid-vapor boundary is continuously moving due to evaporation. The liquid fraction in the outer control volume $dV_o$ during time step $dt$ can be approximated as:

$$\chi \cong 1 - \frac{4\pi r_o^2 \dot{m}'' dt}{\rho_c dV_o} \tag{13}$$

For $0 \leqslant \chi \leqslant 1$, the boundary control volume can be resized as:

$$dV_o' = \chi dV_o \tag{14}$$

Taking the outer control volume to be the $n$th control volume, the updated outer boundary radius can then be obtained from

$$r_o'^3 = r_o^3 \chi + r_{o-1}^3 (1 - \chi) \tag{15}$$

If $\chi < 0$, the entire $n$th control volume has turned into vapor, and the outer boundary would be represented by the $n-1$ control volume.

## 3 Feasibility Study

From a manufacturing point of view, it would be interesting to know whether plasma processing is capable of producing particulate-reinforced metal-matrix composite coatings out of metal-coated powder particles. The problem boils down to whether these particles arrive at the target with the coating molten but not excessively evaporated, and the base retained solid. This

particle state will be referred to as ideal. In order to investigate this, a set of conventional plasma spraying conditions will be assumed, as an input to the developed model, to compute the state of the coated particles at the end of the flight. If this typical set of plasma conditions is found capable of producing the ideal particle state over a range of particle sizes and base/coating relative amounts, then it can be concluded that plasma spray is a feasible process for producing MMC coatings. In other words, if a ''size window'' for processing the commercially available coated particles exists, then theoretically the operating conditions could be adjusted to achieve processing within this window.

**3.1 Input Data.** *Plasma Spray Conditions.* Atmospheric argon plasma was considered. The centerline temperature and velocity distributions for a free argon plasma jet reactor were interpolated from the data presented by Huang et al. [17] at 400 amps. Thermal properties of the plasma such as thermal conductivity, density, and specific heat as a function of plasma temperature were obtained from Chen et al. [18]. Viscosity data for argon plasma were taken from Chen et al. [19].

Initially, the particle was assumed to be at $T_i = 300$ K and to be injected at the plasma nozzle exit with an axial injection component of 10 m/s. The flight distance was taken to be $L = 0.05$ m.

*Particle Data.* The particle outer radius for the coated particles considered was varied in the range $10\ \mu\text{m} < R_o < 30\ \mu\text{m}$. The interface radius $R_i$, which defines the interface between the base and the coating (and therefore the base/coating relative amounts), was also varied in the range $0.2R_o < R_i < 0.8R_o$.

The properties of the two ceramic bases considered, WC and SiC, were taken from Touloukian and Buyco [20], and Shackelfold and Alexander [21], and are given in Table 1. The properties of the three coating materials considered, Co, Al, and Ni, were taken from Touloukian and Buyco [20], and Alfa Aesar [22], and are given in Table 2.

**3.2 Model Output.** The results presented in this section are for a space step of $dr = 0.1R_o$ and a time step $dt$ such that $dt/dr^2 = 5 \times 10^3$ s/m$^2$ for the SiC-Al particle and $1 \times 10^4$ s/m$^2$ for the other two particles, and were determined to be converged. (These results were compared to the ones for $dr = 0.02R_o$ and were found to be indistinguishable. Note that the relatively coarse grid yields accurate results because temperature gradients are generally small.)

The thermal response of 10-$\mu$m radius WC-Co, SiC-Ni, and SiC-Al particles having interface radius of 8 $\mu$m is shown in Fig. 1 plotted against their location inside the reactor. For this particle size temperature gradients are negligibly small for all three particles and the temperature shown actually stands for surface as well as the interior temperature. The highest temperature is attained by the SiC-Ni particle as nickel has the highest boiling point, followed by the WC-Co and finally by the SiC-Al particle. The temperature response of each particle, except for the SiC-Ni, suggests that the base is retained solid throughout the flight as the temperature attains a peak below the melting point of the base owing to intense evaporation. The case of the SiC-Ni particle was in doubt as the base slightly surpassed the invariant melting point of SiC at 2,818 K for about 100 $\mu$s, attaining a maximum temperature at 2,867 K. As this time scale is most likely inadequate for an invariant melting reaction to be completed, no phase change of the base material was considered. The vaporization radius of the three particles is shown in Fig. 2. Evaporation appears to become significant for all particles at nearly the same location. Although the aluminum coating melted much earlier as compared to the other two coatings, evaporation did not become important any sooner because its boiling point is as high as the other two coatings. The cobalt coating shows the least reduction in volume. It did not actually experience the least evaporative mass loss, but its high density yielded the observed small volume reduction.

The surface temperature of 30-$\mu$m radius WC-Co, SiC-Ni, and SiC-Al particles having interface radius of 24 $\mu$m is shown in Fig. 3 as a function of location in the reactor. For this particle size, temperature gradients in the WC-Co particle were small; however they became important for the other two particles as the silicon carbide base has a relatively low thermal conductivity as compared to tungsten carbide. This figure shows that under the same conditions, the aluminum-coated particle has completely melted at the end of its flight while the other two particles have not. This is shown clearly in Fig. 4, which shows the history of the melting

**Table 1 Base properties**

| | WC | SiC |
|---|---|---|
| $\rho_b$ (kg/m$^3$) | 15,800 | 3,200 |
| $c_b$ (J/kgK) | 306 | 1,340 |
| $k_b$ (W/mK) | 57.5 | 12.1 |

**Table 2 Coating properties**

| | Co | Al | Ni |
|---|---|---|---|
| $\rho_c$ (kg/m$^3$) | 8,920 | 2,700 | 8,900 |
| $c_{sc}$ (J/kgK) | 754 | 1,005 | 553 |
| $c_{lc}$ (J/kgK) | 1214 | 1,277 | 603 |
| $k_{sc}$ (W/mK) | 74.6 | 232 | 71.8 |
| $k_{lc}$ (W/mK) | 74.6 | 107 | 82.5 |
| $T_{melt}$ (K) | 1,768 | 933 | 1,727 |
| $T_{boil}$ (K) | 2,870 | 2,740 | 3,005 |
| $L_{fus}$ (MJ/kg) | 0.26 | 0.40 | 0.30 |
| $L_{evap}$ (MJ/kg) | 6.27 | 10.5 | 6.49 |
| $\varepsilon$ | 0.5 | 0.05 | 0.15 |

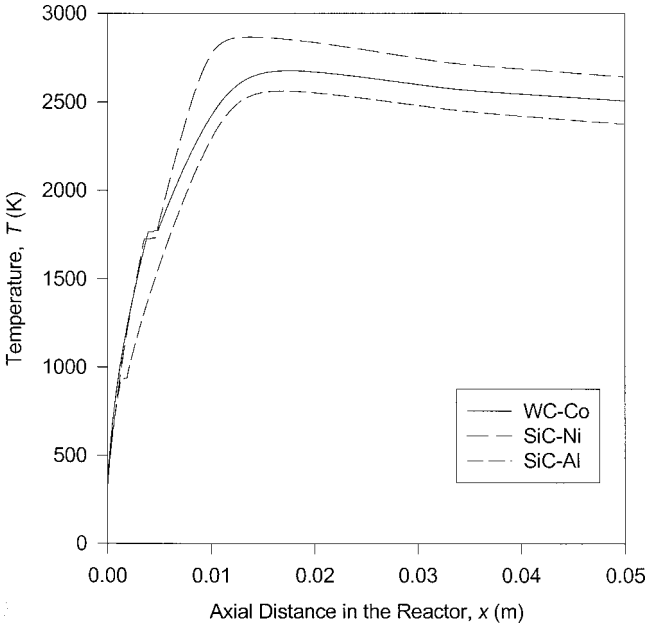


**Fig. 1 Particle surface temperature vs. axial distance in the reactor for a 10-$\mu$m radius particle with $R_i = 0.8R_o$**

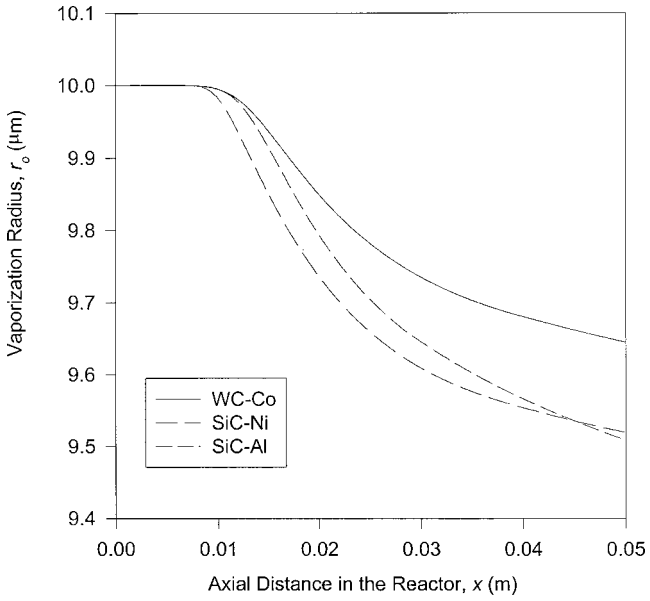


**Fig. 2 Vaporization front vs. particle location in the reactor for a 10-$\mu$m radius particle with $R_i=0.8R_o$**

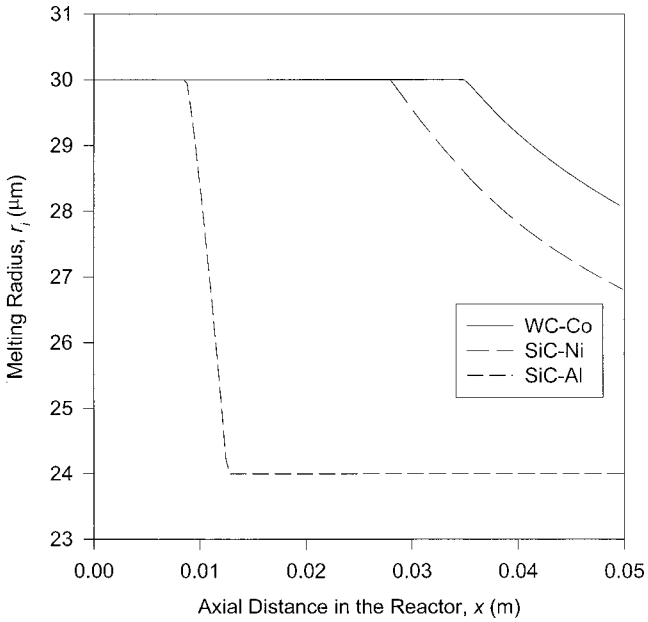


**Fig. 4 Melting front vs. particle location in the reactor for a 30-$\mu$m radius particle with $R_i=0.8R_o$**

interface of each particle during its flight. This figure suggests that the melting interface in the aluminum coating propagated much faster as compared to the other two coatings. This is attributed to the fact that the aluminum coated particle melted earlier when the heat gains from the plasma were significantly greater.

Figures 5, 6, and 7 show the effects of varying the interface radius in the range $0.2 \leqslant R_i/R_o \leqslant 0.8$ on a 20-$\mu$m radius WC-Co, SiC-Ni, and SiC-Al particle respectively. The change in the interface radius has similar effects in the WC-Co and SiC-Ni particles. The quantity $\rho c$ for the base material is less than that for the coating material, so reducing the amount of the base material increases the time constant of the process and therefore slows down the heating of the particle. This effect is reversed for the case of a SiC-Al particle, as the quantity $\rho c$ for the base material is more than that for the coating. Moreover, it should be noted that particles with less coating material, i.e., of greater interface radius, take a shorter time to melt (as a result of a smaller associated latent heat sink) as compared to particles of smaller interface radius. In SiC-Al particles, the effect of latent heat sink opposes the effect of time constant resulting in a smaller overall effect of the interface radius, as compared to the other two particles in which the two effects yield an amplified overall effect.

For the chosen conditions, Fig. 8 represents a map of predicted particle size ranges for given interface radii that would yield the

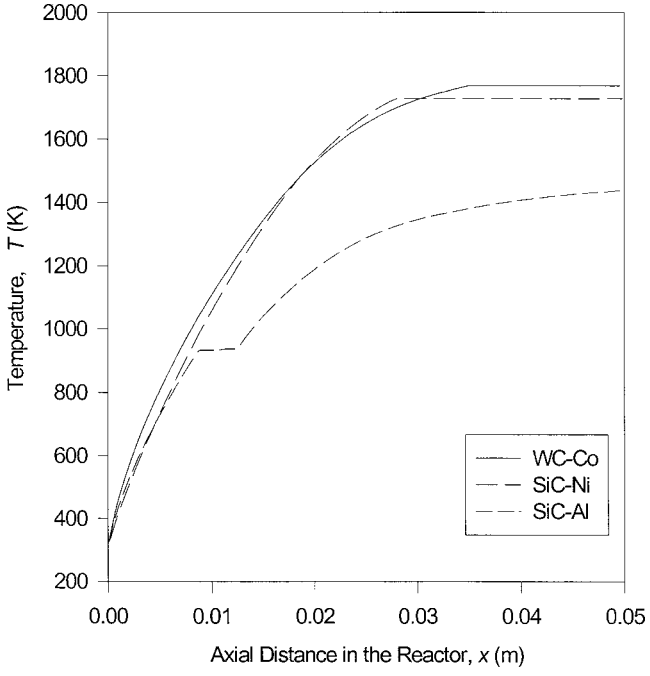


**Fig. 3 Particle surface temperature vs. axial distance in the reactor for a 30-$\mu$m radius particle with $R_i=0.8R_o$**

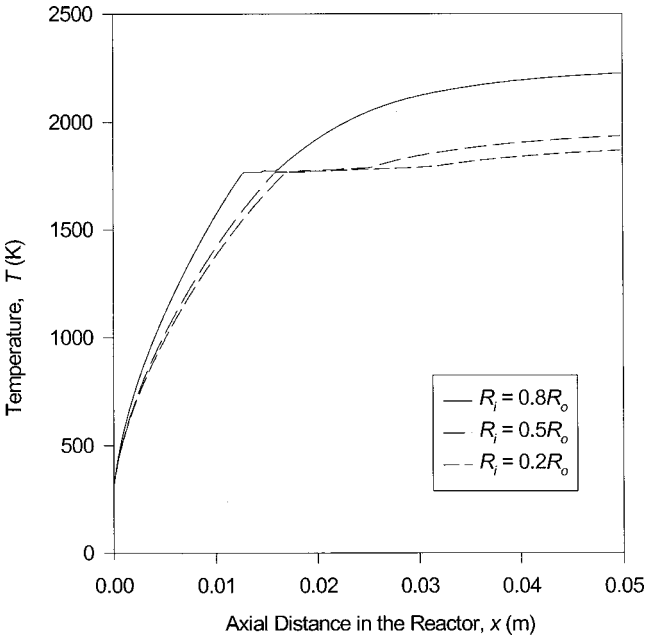


**Fig. 5 Particle surface temperature vs. axial distance in the reactor—the effect of the interface radius on a 20-$\mu$m radius WC-Co particle**

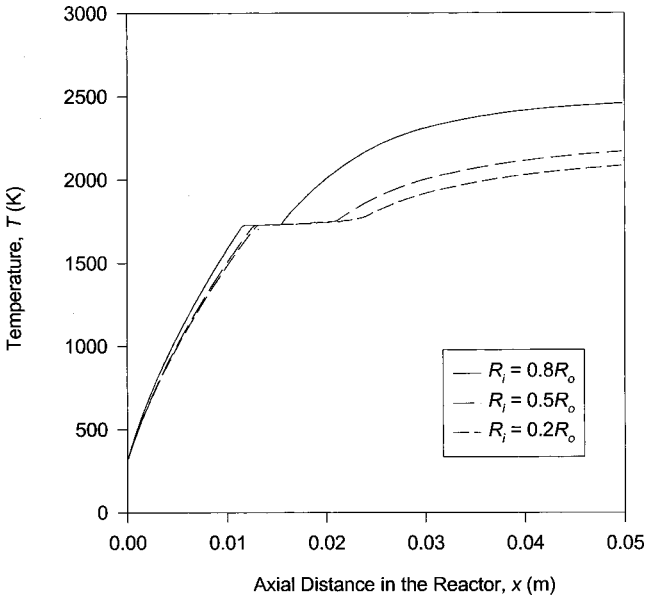


**Fig. 6 Particle surface temperature vs. axial distance in the reactor—the effect of the interface radius on a 20-$\mu$m radius SiC-Ni particle**

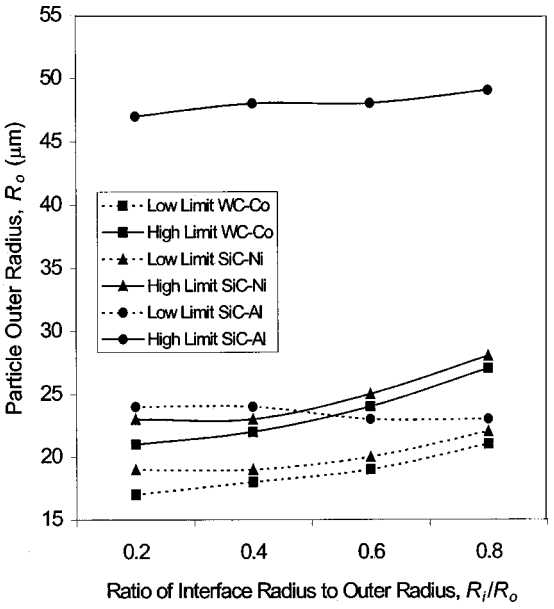


**Fig. 8 Upper and lower limit of particle sizes to attain ideal state prior to impingement**

ideal particle state (i.e., the coating entirely molten with zero evaporative losses) prior to impingement with the substrate. This diagram shows, for a given interface radius, the largest particle size to accomplish complete melting of the coating and the smallest size to completely avoid evaporative losses. As expected, the aluminum-coated particle yielded a much wider range as compared to the other two particles due to the larger difference between melting and boiling points. Moreover, as suggested by Fig. 7, the optimum size range for the SiC-Al particles appears relatively insensitive to the choice of the interface radius as compared to the other two particles. Figure 8 suggests that the given conditions would allow the use of large SiC-Al particles on the order of 50 $\mu$m radius, but no greater than 25 $\mu$m for the other two particles as incomplete melting or no melting would result. On the other hand, fine WC-Co and SiC-Ni particles can be used on the order of 17- and 19-$\mu$m radius respectively without any reduction in volume due to evaporative losses, but no smaller than 24-$\mu$m for SiC-Al.

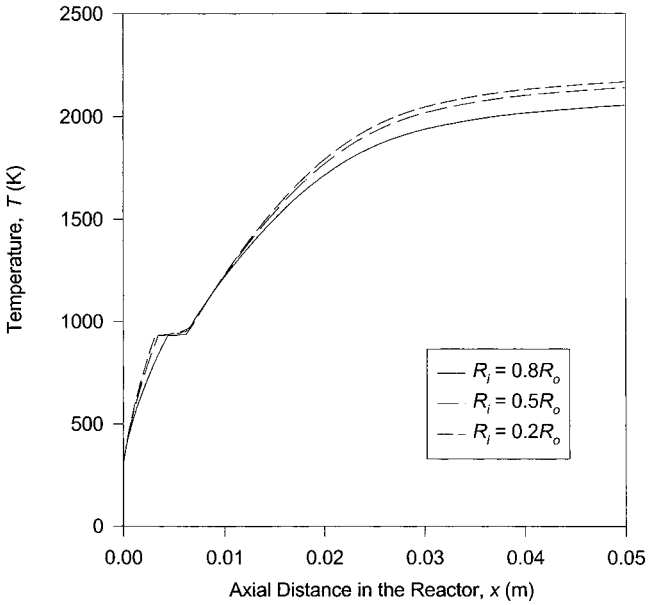


**Fig. 7 Particle surface temperature vs. axial distance in the reactor—the effect of the interface radius on a 20-$\mu$m radius SiC-Al particle**

## Conclusions

In this work, the feasibility of plasma spray processing in producing particulate-reinforced metal-matrix composite coatings is evaluated. A numerical model is presented to analyze the in-flight thermal behavior and physical state of moderate-size particles (10–30 mm radius) in arc-jet DC plasma under low loading conditions. Under the chosen conditions, the particle base was retained solid throughout the flight as the temperature attained a peak below the melting point of the base for all the investigated particles. Reducing the amount of the base material resulted in slowing down the heating of the WC-Co and SiC-Al particles, however, the opposite and less pronounced effect occurred in the SiC-Al particle. The model suggests that for each particle an optimum particle size range exists for a given interface radius that would result in an entirely molten coating without significant evaporative losses. Overall, the model suggests that plasma processing is capable of melting the coating without excessive evaporation while retaining the base in the solid state over a range of particle sizes and interface radii, and hence it could be suitable to develop particulate-reinforced metal-matrix composites.

## Acknowledgments

This work was supported by the Institute of Mechanics and Materials at UCSD and PowderMet, Inc. The valuable discussions with Dr. S. Sharafat, Dr. A. Sherman, and Dr. A. F. Mills are gratefully acknowledged.

## References

[1] Yan, S. P., Mohamed, F. A., Lavernia, E. J., and Srivatsan, T. S., 1995, "Influence of Spray Atomization and Deposition Processing on Microstructure and Mechanical Behaviour of an Aluminum Alloy Metal-Matrix Composite," J. Mater. Sci., **30**, pp. 4726–4736.

[2] Ye, Z., Cheng, H. S., and Chang, N. S., 1996, "Wear Characteristics of Nickel/Silicon Carbide Composite Coating in Lubricated Reciprocating Contacts," Tribol. Trans., **39**, No. 3, pp. 527–536.

[3] Cavaleiro, A., Vieira, T. M., and Lemperiere, G., 1990, "The Structure of Thin

Films Deposited from a Sintered Tungsten Carbide with a High Cobalt Content,'' Thin Solid Films , **185**, pp. 199–217.
[4] Fiszdon, J. K., 1979, ''Melting of Powder Grains in a Plasma Flame,'' Int. J. Heat Mass Transf., **22**, pp. 749–761.
[5] Lee, Y. C., Chyou, Y. P., and Pfender, E., 1985, ''Particle Dynamics and Particle Heat and Mass Transfer in Thermal Plasmas, Part II, Particle Heat and Mass Transfer in Thermal Plasmas,'' Plasma Chem. Plasma Process., **5**, pp. 391–415.
[6] Jog, M. A., and Huang, L., 1996, ''Transient Heating and Melting of Particles in Plasma Spray Coating Process,'' J. Heat Transfer, **118**, pp. 471–477.
[7] Wan, Y. P., Prasad, V., Wang, G.-X., and Sampath, S., 1998, ''Modeling of Powder Particle Heating, Melting and Evaporation in Plasma Spraying Processes,'' *ASME HTD, Vol. 361-4, Proceedings of the ASME Heat Transfer Division, Vol. 4*, pp. 67–77.
[8] Chen, X., and Pfender, E., 1982, ''Unsteady Heating and Radiation Effects of Small Particles in a Thermal Plasma,'' Plasma Chem. Plasma Process., **3**, pp. 293–316.
[9] Pfender, E., and Lee, Y. C., 1985, ''Particle Dynamics and Particle Heat and Mass Transfer in Thermal Plasmas, Part I, The Motion of a Single Particle without Thermal Effects,'' Plasma Chem. Plasma Process., **5**, pp. 211–237.
[10] Young, R. M., and Pfender, E., 1987, ''Nusselt Number Correlations for Heat Transfer to Small Spheres in Thermal Plasma Flows,'' Plasma Chem. Plasma Process., **7**, pp. 211–229.
[11] Demetriou, M. D., Lavine, A. S., and Ghoniem, N. M., 1999, ''Numerical Simulation of Plasma Heating of a Composite Powder Particle,'' *Proceedings of the 5th ASME/JSME Joint Thermal Engineering Conference*, Paper No. AJTE99/6158.
[12] Sujith, R. I., Waldherr, G. A., Jagoda, J. I., and Zinn, B. T., 1996, ''On the Effect of Evaporation on Droplet Drag,'' ASME J. Fluids Eng., **118**, pp. 862–864.
[13] Chen, X., and Pfender, E., 1983, ''Effect of the Knudsen Number on Heat Transfer to a Particle Immersed into a Thermal Plasma,'' Plasma Chem. Plasma Process., **3**, pp. 97–113.
[14] Mills, A. F., 1995, *Heat and Mass Transfer*, Irwin, Chicago.
[15] Sobolev, V. V., Guilemany, J. M., Miguel, J. A., and Calero, J. A., 1995, ''Influence of In-Flight Dissolution Process on Composite Powder Particle (WC-Ni) Behaviour During High Velocity Oxy-Fuel Spraying,'' Surf. Coat. Technol., **81**, pp. 136–145.
[16] Voller, V., and Cross, M., 1981, ''Accurate Solutions of Moving Boundary Problems Using the Enthalpy Method,'' Int. J. Heat Mass Transf., **24**, pp. 545–555.
[17] Huang, P. C., Heberlein, J., and Pfender, E., 1995, ''A Two-Fluid Model of Turbulence for a Thermal Plasma Jet,'' Plasma Chem. Plasma Process., **15**, pp. 25–46.
[18] Chen, X., Chyou, Y. P., Lee, Y. C., and Pfender, E., 1985, ''Heat Transfer to a Particle Under Plasma Conditions with Vapor Contamination from the Particle,'' Plasma Chem. Plasma Process., **5**, pp. 119–141.
[19] Chen, X., Heberlein, J., and Pfender, E., 1996, ''Critical Analysis of Viscosity Data of Thermal Argon Plasmas at Atmospheric Pressures,'' Plasma Chem. Plasma Process., **16**, pp. 635–650.
[20] Touloukian, Y. S., and Buyco, E. H., 1970, *Thermophysical Properties of Matter*, The TPRC Data Series, Vols. 1, 2, 4, 5 and 7, IFI Plenum, New York.
[21] Shackelfold, J. F., and Alexander, W., 1992, *The CRC Materials Science and Engineering Handbook*, CRC Press, Florida.
[22] Alfa Aesar, *Research Chemicals*, 1997–98, Metals and Materials (Company Catalogue).